PROBABILITY DISTRIBUTION OF SURFACE WAVE SLOPE DERIVED USING SUN GLITTER IMAGES FROM GEOSTATIONARY METEROROLOGICAL SATELLITE AND SURFACE VECTOR WINDS FROM SCATTEROMETERS

NAOTO EBUCHI
Institute of Low Temperature Science, Hokkaido University
N19 W8, Kita-ku, Sapporo 060-0819, Japan
Phone: +81-11-706-5470, Fax: +81-11-706-7142
Email: ebuchi@lowtem.hokudai.ac.jp

and

SHOICHI KIZU
Department of Geophysics, Graduate School of Science, Tohoku University
Aoba, Sendai 980-8578, Japan
Email: kizu@pol.geophys.tohoku.ac.jp

ABSTRACT

Probability distribution of the sea surface slope is estimated using sun glitter images derived from visible radiometer on Geostationary Meteorological Satellite (GMS) and surface vector winds observed by spaceborne scatterometers. The brightness of the visible images is converted to the probability of wave surfaces which reflect the sunlight toward GMS in grids of 0.25 deg x 0.25 deg. Slope and azimuth angle required for the reflection of the sun's ray toward GMS are calculated for each grid from the geometry of GMS observation and location of the sun. The GMS images are then collocated with surface wind data observed by three scatterometers. Using the collocated data set of about 30 million points obtained in a period of 4 years from 1995 to 1999, probability distribution function of the surface slope is estimated as a function of wind speed and azimuth angle relative to the wind direction. Results are compared with those of Cox and Munk (1954a, b). Surface slope estimated by the present method shows narrower distribution and much less directivity relative to the wind direction than that reported by Cox and Munk. It is expected that their data were obtained under conditions of growing wind waves. In general, wind waves are not always developing, and slope distribution might differ from the results of Cox and Munk. Most of our data are obtained in the subtropical seas under clear-sky conditions. This difference of the conditions may be the reason for the difference of slope distribution.

KEYWORDS: wind waves, surface slope, sun glitter, scatterometer, Geostationary Meteorological Satellite (GMS), visible radiometer

1. INTRODUCTION

The distribution of the sea surface slopes is of broad interest not only for the physics of wind waves and wave modeling but also for optical models of the ocean surface and ocean color remote sensing. Almost a half century ago, Cox and Munk (1954a, b) derived the probability distribution of surface slope from aerial photographs of the sun's glitter on the sea surface. Their relationship between variance of the surface slope and wind speed has been widely used to model the optical properties of the sea surface. However, their results were deduced from a very limited number of photographs taken under selected conditions.

In the present study we have attempted to estimate the probability distribution of the sea surface slope as a function of wind speed and azimuth angle relative to the wind direction using sun glitter images observed by the Geostationary Meteorological Satellite (GMS) and surface vector winds derived from spaceborne scatterometers, such as the European Remote sensing Satellite (ERS)-1 and ERS-2/Active Microwave Instrument (AMI), and ADvanced Earth Observation Satellite (ADEOS)/National Astronautics and Space Administration (NASA) Scatterometer (NSCAT). High-speed processing of the

GMS data enabled us to obtain a collocated data set for a period of 4.5 years. It is expected that we shall be able to derive a more reliable probability density function under general conditions of wind and waves over the global oceans. Since our data set is obtained under clear-sky conditions with a resolution of an order of 10 km, our results are expected to be directly applicable to optical modeling of the sea surface for ocean color remote sensing. This article is an extended abstract, and this work has been published in full (Ebuchi and Kizu, 2002).

2. DATA

We used the GMS-5/Visible and Infrared Spin Scan Radiometer (VISSR) Histogram Data (Meteorological Satellite Center, 1989) provided by the Japan Meteorological Agency (JMA) for a period of about 4 years from June 14, 1995 to September 30, 1999. The data cover an area of latitude between 60 deg.S and 60 deg.N, and longitude between 80 deg.E and 160 deg.W, with temporal interval of 3 hours. The data store histograms of pixel-wise visible brightness count in grids of 0.25deg. x 0.25deg. (latitude x longitude).

The NSCAT Ocean Wind Products (Level 2.0) provided by the NASA Physical Oceanography Distributed Active Archive Center (PO.DAAC) at the Jet Propulsion Laboratory (JPL), California Institute of Technology, and the ERS-1/2 AMI Off-line Wind Scatterometer Products provided by Centre ERS d'Archivage et de Traitement (CERSAT), Institut Français de Recherche pour l'Exploitation de la Mer (IFREMER), were utilized to collocate with the GMS data. The ERS-1, ERS-2, and NSCAT wind data products cover periods from June 14, 1995 to May 25, 1996, from March 19, 1996 to September 30, 1999, and from September 15, 1996 to June 30, 1997, respectively. The scatterometers are considered to provide with the equivalent neutral wind at a height of 10 m above the sea surface. Several validation studies of these products reported that accuracies of the wind speed and direction observed by these scatterometers are about 2 m/s and 20 deg., respectively.

3. METHOD

Visible brightness counts of all pixels are averaged in grids of 0.25 deg. x 0.25 deg. (latitude x longitude). The mean count is converted to scaled radiance according to the pre-launch calibration table for the radiometer. Aging of the GMS-5/VISSR sensors is compensated by using a method developed by Kizu (2002). Cloud and land area are eliminated, and the brightness of sun glitter on the sea surface is obtained from the images. Cloud areas are detected by grid-averaged infrared brightness temperatures lower than 15 deg.C.

Geometrical parameters, such as the solar elevation and azimuth angles, GMS looking off-nadir and azimuth angles, and slope and azimuth angle of the surface facets required for the reflection of the sun's ray toward GMS, are calculated for the center of each grid from the geometry of GMS observation and location of the sun. The Fresnel reflection coefficient is estimated from the slope angle. The brightness of the visible images is converted to the probability of wave surfaces which reflects the sunlight toward GMS by assuming that the brightness is proportional to the area of sea surface which reflects the sunlight. Only the primary scattering at the sea surface is considered, and scattering from the atmosphere is neglected.

The GMS images are then collocated with surface wind data observed by the three scatterometers. Temporal separation between the GMS and scatterometer observations are limited to within 90 min. Although we tried narrower time windows for the collocation (*e.g.*, 60, 30, and 15 min.), the results showed no significant differences. The scatterometer vector fields of 50 km spatial resolution are linearly interpolated to the grid of 0.25 deg. x 0.25 deg. to be collocated with the GMS data.

Using the collocated data set of about 30 million points obtained in a period of about 4 years from 1995 to 1999, the probability distribution function of the surface slope was calculated as a function of wind speed, azimuth angle relative to the wind direction, and incidence angle in bins of 1 m/s in wind speed, 10 deg. in azimuth angle, and 1 deg. in incidence angle.

4. RESULTS

Figure 1 shows an example of the probability distribution of surface slope in the upwind/ downwind and crosswind directions under wind speed of 7 - 8 m/s. The upper panels show the mean and standard deviation of the probability distribution function (PDF) in arbitrary units, and the lower panels show the number of collocated data points used to calculate the probability distribution. The mean and standard deviation are calculated only where the number of data points exceeded 10. Outlyers which exceed three times the standard deviation were discarded and the mean and standard deviation were recalculated.

The distribution of data points is not uniform, representing the geometry of the sun and GMS observation and prevailing winds. In particular, there are few data points at normal incidence because of the geometrical constraints

of the sun and GMS observation and the geographical location of islands in the western Tropical Pacific.

As expected, the probability decreases with the incidence angle. However, it does not reach zero even at high incidence angles. It is considered that scattering from the atmosphere and diffusive reflectors on the sea surface, such as whitecaps and bubbles, increases the reflection of sunlight and results in overestimation of the probability distribution function, which is assumed to be proportional to the brightness of sun glitter images. Assuming that these effects do not vary greatly with incidence angle, we fitted a Gaussian function with a constant bias to the data as,

$$p(\theta) = a\exp\left(-\tan^2\theta/2\sigma^2\right) + b \qquad (1)$$

where p is the probability density function, θ is the incidence angle, σ is the root-mean-square (rms) slope, and a and b are constants. The values of σ, a, and b are determined by the least square method. Thick lines in Fig. 1 are the fitted curves. The fitted curves represent the dependence of data points on incidence angle very well. No upwind/downwind asymmetry, as reported by Cox and Munk (1954a, b), is discernible, even under high winds.

The variance of the surface slope components are plotted against wind speed in Fig. 2 (circles). Error bars indicate the 95% confidence interval using the least-squares fit to the data by Eq.(1). Thick lines represent the linear regression line on the data. Thin solid and broken lines represent formulae proposed by Cox and Munk (1954a, b) for clean and slick surfaces, respectively. Although the wind speed dependence of the crosswind slope component agrees well with that of Cox and Munk (1954a, b), the upwind/ downwind component is much lower. The surface slope estimated by the present method shows a narrower distribution and much less directivity relative to the wind direction than that reported by Cox and Munk (1954a, b).

5. DISCUSSION

The results presented in the preceding section showed that the probability distribution of the surface slope has less asymmetry relative to the wind direction than that revealed by Cox and Munk (1954a, b). One possible reason is the difference in spatial resolution of the observation techniques. Cox and Munk (1954a, b) took photographs of the sun glitter from aircraft flying at an altitude of 2000 ft (600 m), and the typical spatial scale of their observation is expected to be of the order of 1 - 10 m. By contrast, the spatial resolution of our data set is 0.25 deg. As suggested by Strong and Ruff (1970), variability of wind directions in the relatively large area over 0.25 deg. x 0.25 deg. to some extent may smear the directivity of slope distribution relative to the wind direction.

It is also expected that Cox and Munk (1954a, b) obtained their data under growing wind wave conditions, which is in equilibrium with the wind. In general, wind waves are not always developing, and the slope distribution might differ from their results (*e.g.*, Donelan and Pierson, 1987). This difference in conditions may be the reason for the difference of slope distribution.

Figure 3 shows (a) a histogram of wave age and (b) a comparison of wind and wave directions of the data utilized by Cox and Munk (1954a, b). The wave age is defined by the ratio of phase speed of the dominant wave and the friction velocity of the air. Except for four data points, the directions of wind and waves agree with each other, and the wave age is lower than 30. This implies that the data of Cox and Munk were obtained under conditions of growing to fully-developed wind waves. According to Bailey *et al.* (1991), most of the wind and wave data observed under forcing of local wind show values of the wave age under 25. To the contrary, most of the present data were obtained in a region of subtropical high. It is expected that swell is dominant in this region rather than growing wind waves. In order to examine the difference of conditions of wave growth between the data sets of Cox and Munk and the present study, we use the non-dimensional waveheight defined as,

$$\hat{H} = gH_{1/3}/U_{10}^2 \qquad (2)$$

where g is the acceleration of gravity, $H_{1/3}$ is the significant wave height, U_{10} is the wind speed at a height of 10 m above the sea surface. The relationship between the non-dimensional waveheight and fetch has been investigated for the purposes of wave modeling. For wind waves, the non-dimensional waveheight increases with the non-dimensional fetch and is saturated to 0.3 (Wilson, 1965; Hasselmann et al., 1980; Ebuchi *et al.*, 1992; Ebuchi, 1999). The significant waveheights observed by TOPEX/ POSEIDON altimeter along the satellite subtracks were averaged in grids of 0.25 deg. X 0.25 deg. and were colloca-

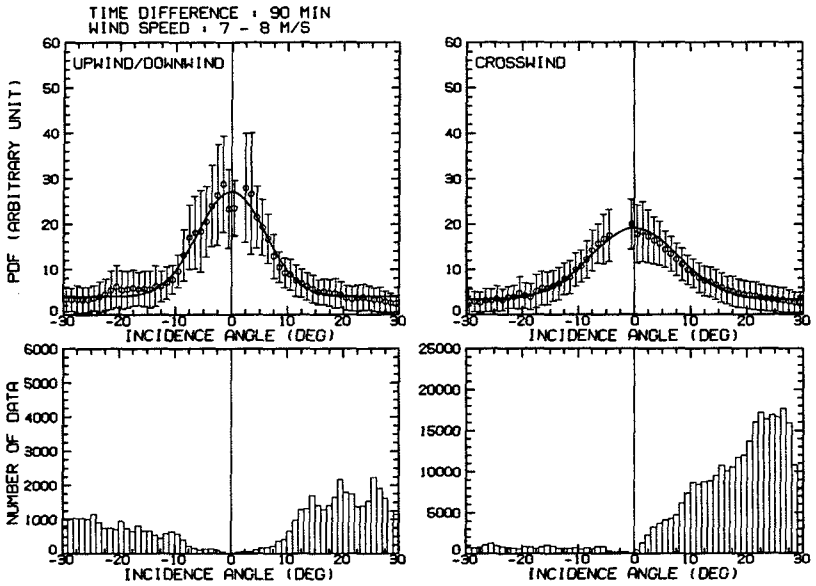

Figure 1. Probability distribution of wave slope (upwind/downwind and crosswind directions) in an arbitrary unit (upper panels), and the number of collocated data points used to calculate the probability distribution (lower panels) at wind speed of 7 - 8 m/s.

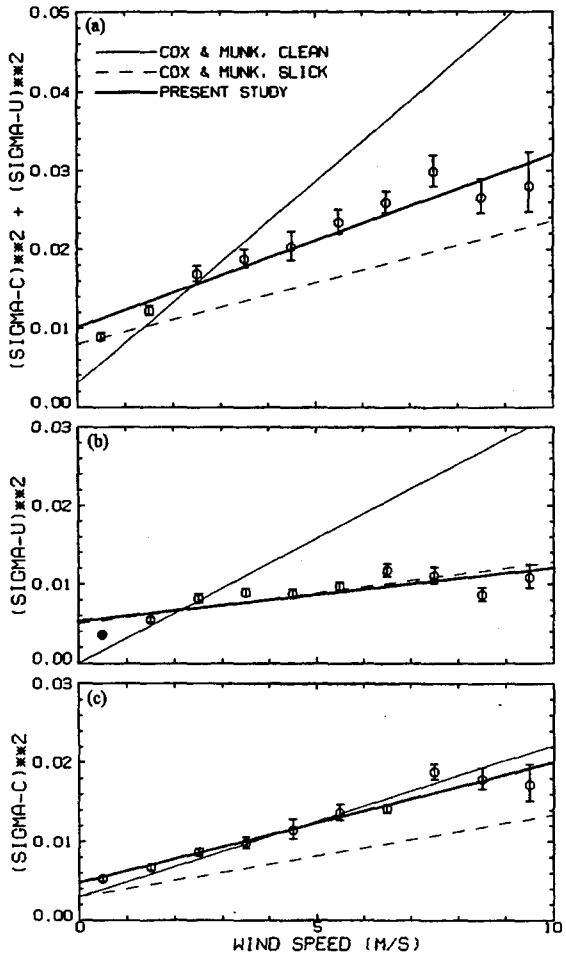

Figure 2. Mean square slope components and their sum as functions of wind speed. (a) Total slope, (b) upwind/downwind, and (b) crosswind components. Error bars indicate 95% confidence intervals. Thick lines represents the linear regression line on the data. Thin solid and broken lines represent formulae proposed by Cox and Munk (1954a, b) for clean and slick surfaces, respectively.

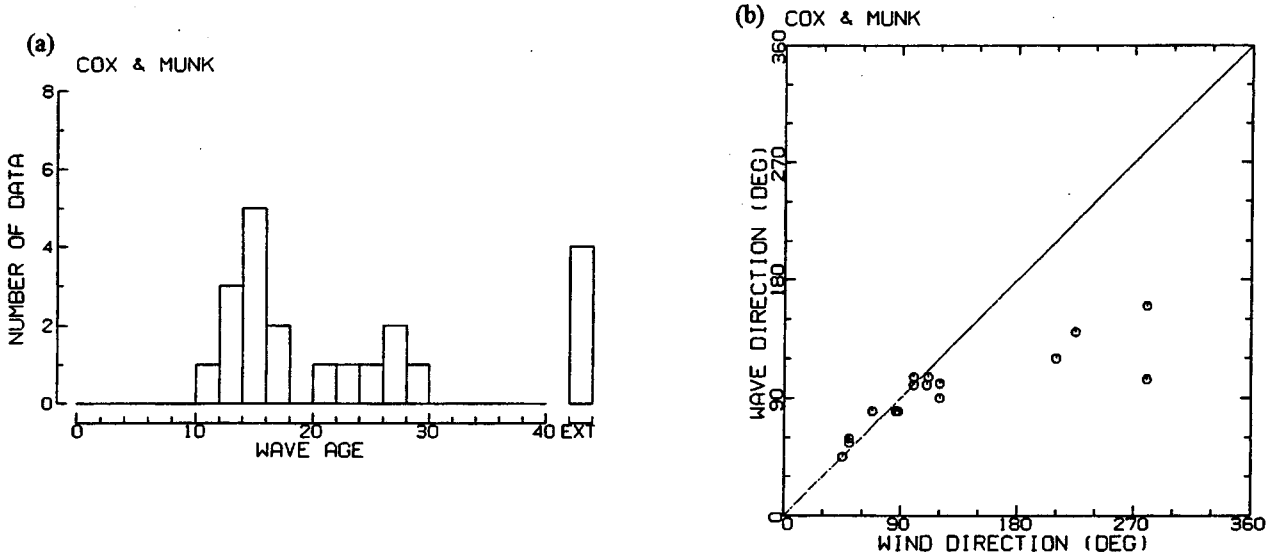

Figure 3. (a) Histogram of wave age and (b) comparison of wind and wave directions of the data utilized by Cox and Munk (1954a, b). "EXT" implies values of wave age greater than 40.

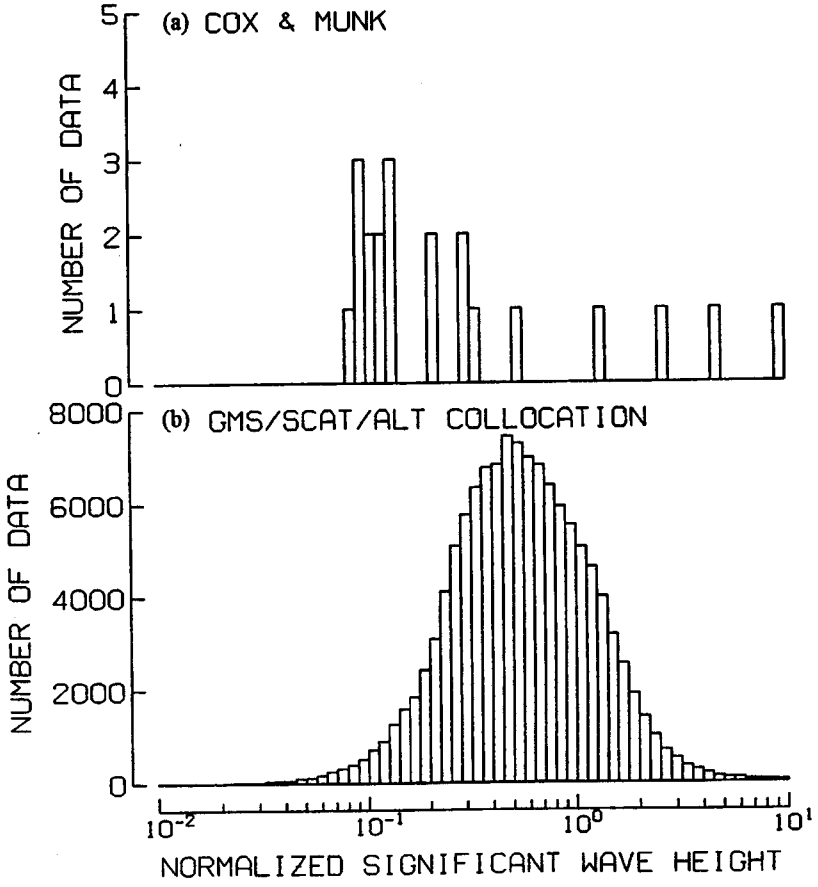

Figure 4. Comparison of histograms of non-dimensional significant waveheight of the data utilized by (a) Cox and Munk (1954a, b), and (b) the present study.

ted allowing time difference within 90 min. About 122,000 data points were collocated. Figure 4 shows histograms of the non-dimensional significant waveheight of the data utilized by Cox and Munk (1954a, b) and the present study. Most of the Cox and Munk data points have values of the non-dimensional wave height around 0.1, implying that waves are growing under winds. In contrast to the data of Cox and Munk, a large portion of the present data set has a value of the non-dimensional significant waveheight larger than 0.3, implying that swells are dominant and waves are not expected to be in equilibrium with winds. It is considered that these differences in the conditions of wave growth caused the difference in slope distribution shown in Fig. 2. Swells propagating from various directions, which are independent of the local wind direction, result in the isotropic distribution of the surface slope. We believe the present data set represents a more general condition of wind waves over the global oceans than the limited data set of Cox and Munk (1954a, b). Bailey *et al.* (1991) discussed the relationship between the shape of wind waves and wave age. They concluded that younger wind waves are steeper and more asymmetric. Older waves approach a symmetric, sinusoidal form. This may explain the difference in upwind/ downwind asymmetry of the surface slope. The results of the present study deduced from data obtained under a clear sky can be directly applicable to modeling the sea surface for optical remote sensing of the ocean, such as ocean color observations.

REFERENCES

Bailey, R.J., I.S.F. Jones, and T. Toba, 1991, The steepness and shape of wind waves. *J. Oceanogr. Soc. Japan*, **47**, 249-264.

Cox, C. and W.H. Munk, 1954a, Statistics of the sea surface derived from sun glitter. *J. Mar. Res.*, **13**, 198-227.

Cox, C. and W.H. Munk, 1954b, Measurements of the roughness of the sea surface from photographs of the sun's glitter. *J. Opt. Soc. Am.*, **44**, 838-850.

Donelan, M.A. and W.J. Pierson, 1987, Radar scattering and equilibrium ranges in wind-generated waves with application to scatterometry. *J. Geophys. Res.*, **92**, 4971-5029.

Ebuchi, N., 1999, Growth of wind waves with fetch in the Sea of Japan under winter monsoon investigated using data from satellite altimeters and scatterometer. *J. Oceanogr.*, **55**, 575-584.

Ebuchi, N., H. Kawamura, and Y. Toba, 1992, Growth of wind waves with fetch observed by the Geosat altimeter in the Japan Sea under winter monsoon. *J. Geophys. Res.*, **97**, 809-819.

Ebuchi, N., and Kizu, 2002, Probability distribution of surface wave slope derived using sun glitter images from geostationary meteorological satellite and surface vector winds from scatterometers. *J. Oceanogr.*, **58**, 477-486.

Hasselmann, D.E., M Dunkel, and J.A. Ewing, 1980, Directional wave spectra observed during JONSWAP 1973. *J. Phys. Oceanogr.*, **10**, 1264-1280.

Kizu, S., 2002, An estimation of degradation of VISSR visible sensors aboard GMS-3, GMS-4, and GMS-5 during 1987-1999. *Int'l J. Remote Sens.* (in press).

Meteorological Satellite Center, 1989, The GMS User's Guide (2nd ed.). Japan Meteorol. Agency, Tokyo, Japan, 222p.

Strong, A.E. and I.S. Ruff, 1970, Utilizing satellite-observed solar reflections from the sea surface as an indicator of surface wind speeds. *Remote Sens. Environ.*, **1**, 181-185.

Wilson, B.W., 1965, Numerical prediction of ocean waves in the North Atlantic for December, 1959. *Dtsch. Hydrogr. Z.*, 18 114-130.